Available online at www.sciencedirect.com
SCIENCE DIRECT®
ELSEVIER
Earth and Planetary Science Letters 218 (2004) 451–462
EPSL
www.elsevier.com/locate/epsl

Thermodynamic models for eclogitic mantle lithosphere[1]

E.D. Ghent [a,*], G.M. Dipple [b], J.K. Russell [b]

[a] *Department of Geology and Geophysics, The University of Calgary, Calgary, AB, Canada T2N 1N4*
[b] *Research Institute for Geochemical Dynamics, Earth and Ocean Sciences, The University of British Columbia, Vancouver, BC, Canada V6T 1Z4*

Received 30 March 2003; received in revised form 29 July 2003; accepted 11 November 2003

Abstract

Cratonic mantle eclogite xenoliths occur with diamond-bearing kimberlite. The modes and mineral compositions of eclogite contain important information on their origin, physical-chemical conditions of formation, and their geophysical properties. We have used the pseudosection option of the program PERPLEX to explore how mineral assemblage, abundance, and composition vary with bulk composition, temperature (T) and pressure (P). We considered a range of protolith compositions, including: fresh unaltered basalt, altered seafloor basalt, cumulates resulting from high-pressure crystallization of basaltic melts, and metasomatically altered (SiO_2-depleted) basalt. Stable mineral assemblages and associated geophysical properties for each protolith were calculated at P–T conditions found along the mantle geotherm for the Slave craton. At depths greater than 90 km, the predicted modal mineralogy of eclogite for all protoliths changes little along the geotherm. Within the diamond stability field of cratonic mantle, eclogite has a single mineral assemblage that reflects protolith composition. We recognize three basic classes: (1) a silica-oversaturated assemblage indicated by the presence of coesite, (2) a silica-saturated assemblage distinguished by the absence of coesite and olivine, and (3) a silica-undersaturated assemblage containing olivine. Within the diamond stability field for the Slave geotherm, kyanite is stable only in extremely Al-enriched protoliths. Most kimberlite-hosted eclogite belongs to class 2 and our results show that it cannot derive from either fresh or altered seafloor basalt. We suggest an origin involving mantle metasomatism (SiO_2 depletion) operating on subducted basalt although we cannot rule out an origin from cumulates of metaluminous, subalkaline magmas. Predicted seismic velocities of model eclogite are higher than corresponding velocities for peridotite and most crustal rocks and therefore may be distinctive in regional seismic surveys. However, the only class of eclogite that could be distinguished from seismic data is the oversaturated assemblage (class 1). The quartz–coesite transition produces sharp changes in both P and S wave velocities at depths of about 90 km along the ambient mantle geotherm.
© 2003 Elsevier B.V. All rights reserved.

Keywords: cratonic mantle eclogite; geotherm; stable mineral assemblages; P–T pseudosections; geophysical properties

1. Introduction

Cratonic mantle eclogite xenoliths occur in diamond-bearing kimberlite. Eclogite is likely distributed throughout cratonic mantle lithosphere (e.g.,

* Corresponding author.
E-mail address: ghent@ucalgary.ca (E.D. Ghent).

[1] Supplementary data associated with this article can be found at doi:10.1016/S0012-821X(03)00678-2

0012-821X/03/$ – see front matter © 2003 Elsevier B.V. All rights reserved.
doi:10.1016/S0012-821X(03)00678-2

[1,2]), but geobarometers are generally lacking for mantle-type eclogite. Study of these rocks can provide information on: (1) the protolith, origins, and pressure (P) and temperature (T) conditions for mantle eclogite, and (2) the variation in geophysical properties of eclogite with depth within mantle lithosphere.

We have modeled eclogite mineralogy, using the thermodynamic database of Holland and Powell [3] and the program PERPLEX of Connolly [4] to compute P–T pseudosections (e.g., [3]). These diagrams illustrate eclogite phase relationships as a function of P and T for a series of specific bulk compositions. We have: (1) predicted mineral composition, abundance, and physical properties of eclogite along a calculated mantle geotherm for a variety of protolith compositions; (2) discussed the origins and/or P–T formation conditions of eclogite and their relationships to diamond stability; and (3) computed approximate geophysical properties of eclogite at mantle conditions from the model mineral assemblages.

Our conclusions are threefold. First, along the cratonic mantle geotherm, we predict a simple, common mineralogy of garnet (Grt)+clinopyroxene (Cpx) ± subordinate amounts of coesite (Coe), orthopyroxene (Opx), olivine (Ol), ilmenite (Ilm) or rutile (Rt) for a wide range of protolith compositions. Second, we identify minerals that are important monitors of P–T conditions and bulk composition. These minerals (e.g., Coe) can also have effects on the geophysical properties of eclogite. The latter attribute may allow for mapping discrete masses of eclogite within mantle lithosphere. Finally, we show that typical basalt compositions are not viable protolith compositions to mantle eclogite (see, e.g., [5]).

2. Thermodynamic models for phase assemblages

Mantle eclogite generally contains the assemblage Cpx–Grt–Rt. Other subordinate phases include kyanite and orthopyroxene. SiO_2 polymorphs are generally lacking. Our computations used the model chemical system: Na_2O–CaO–MgO–FeO–Al_2O_3–SiO_2–TiO_2 and we considered the following *phases*: quartz (Qtz), Coe, kyanite (Ky), ilmenite, rutile and the following *phase components* in solid solutions: anorthite, high albite, diopside, hedenbergite, Ca-tschermak pyroxene, Mg-tschermak pyroxene, Fe-tschermak pyroxene, jadeite, enstatite, ferrosilite, forsterite, fayalite, pyrope, almandine, and grossular. Solution models are from the PERPLEX file, solut.dat (see on-line database). The protolith compositions used in our calculations span the range of anhydrous basalt compositions and are listed in the on-line database. All protolith compositions were normalized on an anhydrous basis after converting all iron to ferrous iron and dropping the oxides: MnO, K_2O, and P_2O_5.

2.1. *Calibration of* P–T *pseudosections*

The results of high-pressure experiments from Green and Ringwood [6] provide a validation of our thermodynamic model. Their experimental data provide approximate modes and mineral compositions produced in samples of alkali olivine basalt (AOB) at controlled P–T conditions. The experiments covered a pressure range of 10^5 Pa to 3 GPa at 1100°C. We have used PERPLEX to calculate the stable minerals and the model assemblages accurately reproduce the sequences of mineral occurrence and disappearance in P–T space (Fig. 1). Our model correctly predicts with increasing pressure the appearance of garnet, the disappearance of olivine, the disappearance of plagioclase and the appearance of rutile. The predicted (model) phase assemblages at specific P–T (1100°C and 3 GPa) conditions differ slightly from the experiments. Model olivine is stable up to 1.4 GPa whereas olivine disappears in the experiments at about 1 GPa. Model plagioclase disappears and rutile crystallizes at pressures approximately 0.4 GPa higher than observed. Our model predicts the stable coexistence of ilmenite and rutile at high pressure whereas Green and Ringwood [6] report only rutile in their experimental charges. In summary, our model captures the mineralogy and pattern of the P–T phase relationships well except for the nature of the Fe–Ti oxides and small variations (< 0.5 GPa) in the pressure of specific phase boundaries.

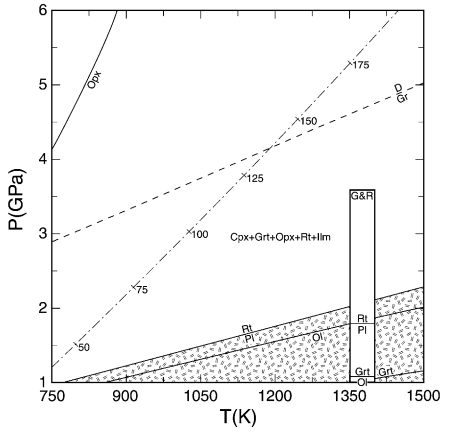

Fig. 1. Calibration of PERPLEX model calculations against experimental phase equilibrium results from Green and Ringwood [6] for AOB at mantle *P–T* conditions. Solid lines are calculated and show predicted changes in mineral assemblage across phase boundaries or narrow regions (divariant) of *P–T* space defined by the loss (e.g., plagioclase) or first appearance (e.g., garnet) of specific minerals. Shaded region is predicted plagioclase stability field. Phase assemblages produced in high-*P–T* experiments are summarized schematically in vertical column (G and R; see text). Also shown are diamond–graphite transition boundary (dashed) and the Slave geotherm (dash-dot; labels indicate depth in km) [1,8]. All mineral abbreviations are taken from Kretz [7] except D (diamond) and Coe (coesite; Fig. 2).

3. Thermodynamic phase relationships in basaltic compositions

The protolith compositions include mid-ocean ridge basalt (MORB), AOB, tholeiite basalt (THL), high-Al basalt (HAB), and ankaramite (ANK). *P–T* pseudosections were prepared for each protolith for a temperature and pressure range of 750–1500 K and 1–6 GPa, respectively. A representative example for MORB is presented in Fig. 2; those interested in the detailed examination of pseudosection diagrams for all five basaltic protoliths are directed to an on-line database.

The overall mineralogy predicted for mantle eclogite is relatively simple (e.g., Fig. 2). Over the range of *P–T* conditions explored, the minerals Grt, Cpx, plagioclase (Pl), Opx, Ol, and Ilm can be produced from all five protoliths (mineral abbreviations after Kretz [7]). In detail, however, there are substantial mineralogical differences between protoliths based on specific minerals (i.e., Ky, Qtz) or the *P–T* conditions that support specific minerals (i.e., Ilm, Ol).

All protoliths support the *P–T* occurrence of the minerals Cpx+Grt over a wide *P–T* range. Opx is generally stable in all protoliths at high-*T* and low-*P* conditions, although in ANK Opx has a lower pressure limit, and in AOB Opx is stable at all model *P–T* conditions. Rt is stable over a wide range of *P–T* conditions for all protoliths except ANK. Ol and Ilm are practically absent in all protoliths; where present they are restricted to high-*T*, low-*P* conditions. Typically, olivine is replaced by Opx and Ilm by Rt. ANK is an exception; Ol is stable and replaces Opx at higher pressures and Ilm replaces Rt over all *P–T* conditions. The occurrence and stability of SiO_2 polymorphs Qtz and Coe is strongly controlled by bulk composition. Silica polymorphs are stable at all *P–T* conditions in HAB and in MORB and THL except at very high-*T* and low-*P* conditions. In AOB Qtz is produced at high pressure, near the Pl out-reaction. Neither Qtz nor Coe is present in ANK.

The largest stability field for Ky occurs in HAB followed by MORB (Fig. 2) and THL; silica-undersaturated compositions lack Ky. The *P–T*

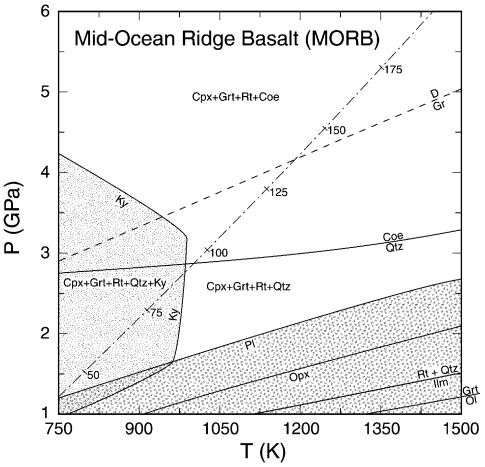

Fig. 2. Calculated *P–T* pseudosection phase diagrams (e.g., PERPLEX) summarizing the phase relationships in eclogite in cratonic lithospheric mantle and deriving from a protolith composition equivalent to MORB. Major lines and symbols are as explained in Fig. 1; shaded fields denote the *P–T* stability fields for plagioclase (coarse) and kyanite (fine).

range over which Ky is stable in these protoliths is restricted. In normal metaluminous compositions Ky is stable at temperatures below 975 K and pressures below 4.2 GPa (the latter only at $T < 800$ K). HAB increases the stability field to temperatures below 1200 K and pressures below 4.7 GPa. The presence of Ky-bearing eclogite (e.g., [1,2]), therefore, offers constraints on the protolith composition and P–T conditions. Unless the protolith is exceptionally high in Al_2O_3, Ky-eclogite must derive from the shallow mantle (e.g., < 3 GPa).

4. Eclogite on the geotherm

The phase relationships for model eclogites shown in these pseudosections (Fig. 2 and online database) are for a P–T range that is substantially greater than found in cratonic mantle litho-

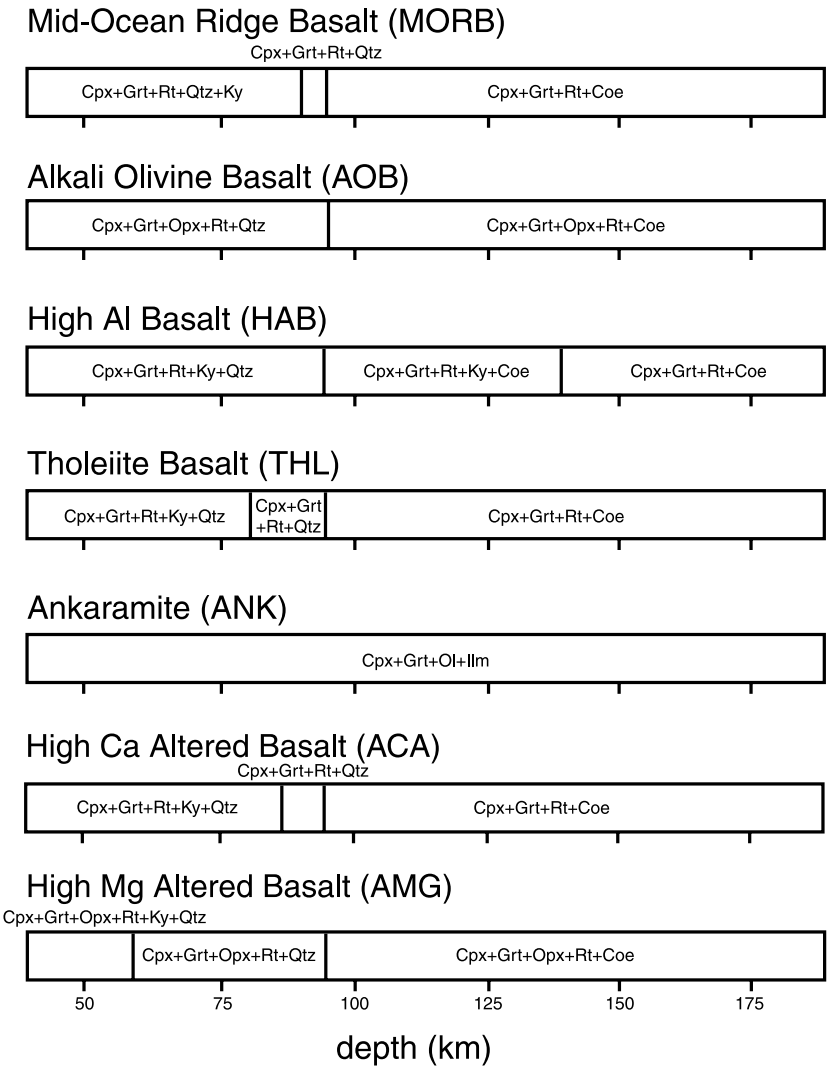

Fig. 3. Mineral assemblages of eclogite calculated for different protolith compositions (e.g., PERPLEX) at P–T conditions on the geotherm for the Slave mantle lithosphere. Mineral assemblages are are plotted against depth (km) and protoliths include: MORB, HAB, AOB, THL, and ANK, as well as compositions representing high-Ca and high-Mg altered seafloor basalt. The mineral assemblages predicted at depths greater than 100 km are used to define classes of eclogite (see Table 1).

sphere. We now focus on the variations in eclogite properties associated with moving each protolith composition along the *P–T* trajectory defined by mantle geotherm for the Slave craton (dashed line in Fig. 2; e.g., [1,2,8,9]). Clearly, another geotherm cutting across the pseudosection shown in Fig. 2 would describe an alternative sequence of stable mineral assemblages.

4.1. Mineralogic variations

The intersection of the model geotherm with the calculated *P–T* phase relationships greatly restricts the ranges of mineralogy produced by individual protoliths. For example, for all protoliths at *P–T* conditions on the mantle geotherm, Ky occurs within the graphite stability field and cannot coexist with diamond (e.g., Fig. 2). Diamondiferous Ky-eclogite would only result from protoliths that are more aluminous than HAB. It is important to realize that cooler geotherms (higher *P*/*T* ratios) that characterize ultra-high-pressure metamorphic belts would support Ky within the diamond stability field [10].

Fig. 3 summarizes the mineralogical variations for each protolith associated with increasing *P–T* conditions defined by the Slave geotherm. We have used the different mineral assemblages of eclogite within the diamond stability field (Fig. 3) to recognize three classes of mantle eclogite (see Table 1). For example, class 1 eclogite has the critical assemblage Cpx+Grt+Coe (Table 1) and results from MORB within the diamond stability field (Figs. 2 and 3). Within the diamond stability field, along the Slave geotherm MORB, HAB and THL all contain Cpx+Grt+Rt+Coe (class 1; Table 1). AOB contains the same assemblage plus Opx (class 1b), and ANK consists of Cpx+Grt+Ol+Ilm (class 3). The implication is that for each basaltic protolith composition, such as MORB, diamondiferous eclogite will have one unique mineral assemblage.

4.2. Mineral modes and rock properties

We have computed the abundance and composition of minerals within each *P–T* field using the WERAMI routine in PERPLEX. The variations in mineral abundance and composition with depth along the Slave geotherm are available as an online database. At depths greater than 40 km, modes of the different protoliths change very slowly along the Slave geotherm. With increasing depth (>40 km) the following patterns are observed: (a) Ky abundance strongly decreases, (b) modal Opx, if present, decreases, and (c) Grt content increases slightly. Our calculations show a slight but consistent increase in pyrope content of Grt with increasing pressure. The jadeite content of Cpx also increases with depth except in AOB and ANK where alumina substitutes into Opx with increasing pressure. The mineral abundances at specific *P–T* conditions are used to compute the expected density and heat capacity of the model eclogite. Both properties increase with depth, however, heat capacity shows stepwise increases that correspond to substantial changes in modal mineralogy (e.g., loss of Ky). These same datasets form the basis for computing seismic velocities and Poisson ratios of eclogite for the different protoliths along the geotherm (see below).

Table 1
Classification of mantle eclogite mineral assemblages based on phase relationships (see Fig. 4) computed for specific *P–T* conditions (1168 K, 4 GPa) found on the ambient cratonic mantle geotherm

	Cpx	Grt	Opx	Ol	Ky	Coe	Protoliths (Fig. 3)
Class 1	X	X				X	THL, MORB, HAB, ACA
Class 1b	X	X	X			X	AOB, AMG
Class 1c	X	X			X	X	
Class 2	X	X					
Class 2b	X	X	X				
Class 2c	X	X			X		
Class 3	X	X		X			ANK
Class 3b	X	X	X	X			

4.3. Classes of eclogite

Fig. 4 provides a schematic portrayal of the possible phase relationships in eclogite as a function of silica and alumina activities. The calculations were done at 1168 K and 4 GPa as a function of the activity of SiO_2, using Coe as a standard state and the activity of Al_2O_3, using corundum (Co) as a standard state [11]. In all calculations unit activities of all phases were assumed and the topology of Fig. 4 is only qualitatively applicable to eclogites. Fig. 4 serves to show how variations in the chemical potentials or activities, of SiO_2 and Al_2O_3, produce different mineral assemblages at constant P and T.

The most commonly observed eclogite contains Cpx+Grt (class 2) and the corresponding field is denoted by the shaded region of the phase diagram (Fig. 4). Eclogite containing other phases, (e.g., Co or Ky), are less common and reflect differences in bulk chemistry as well as P/T. For example, along cooler geotherms such as those that characterize ultra-high-pressure belts, class 1c or 2c eclogites can result from metaluminous compositions and can contain diamonds (e.g., Fig. 2 [10]). In order to produce class 1c or 2c eclogite along a cratonic mantle geotherm requires protolith compositions that are substantially more aluminous than HAB. The common occurrence of Coe in our models for diamondiferous eclogite (classes 1, 1b and 1c) is inconsistent with observations on kimberlite-hosted eclogite, and is the motivation for examining alternative compositions as protolith to mantle eclogite.

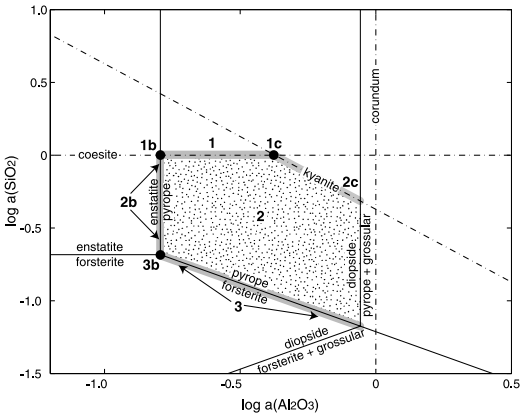

Fig. 4. Log activity diagram showing phase relationships in CaO–MgO–Al_2O_3–SiO_2 system at specific upper mantle P–T conditions (1168 K, 4 GPa). Mineral stability fields are used to establish classes of eclogite based on mineral assemblage (cf. Table 1 and Fig. 3). Class 1 assemblages are silica-oversaturated (Coe present) and typical of basaltic protoliths (e.g., MORB, HAB). Class 1b is a subset of class 1 which contains Opx. Class 2 assemblages are silica-saturated and typical of natural eclogites; Coe is absent and they contain Cpx+Grt ± Opx. Class 3 assemblages result from high-Mg and silica-poor protoliths (e.g., ANK) at upper mantle conditions (cf. Fig. 3) and comprise Cpx+Grt in association with Ol ± Opx. Ky is rare in cratonic mantle lithosphere and would be indicative of highly aluminous protoliths that are silica-oversaturated (class 1c: Cpx+Grt+Ky ± Coe) or silica-saturated (class 2c: Cpx+Grt+Ky). All classes may contain Ilm and/or Rt.

5. Other eclogite protolith compositions

In this section we examine the consequences of non-basaltic protolith compositions on the mineralogy and physical properties of mantle eclogite. We apply our same model calculations to an array of compositions that might be produced by: (a) seafloor alteration of MORB, (b) cumulates from high-pressure magmatic crystallization of basaltic magma, and (c) metasomatic loss of SiO_2 from basalts.

5.1. Seafloor altered basalt protoliths

We have used two average compositions of seafloor altered basalt [12] to model eclogite formation from altered seafloor crust. P–T pseudosections are presented for high-Ca and high-Mg end-member compositions derived from alteration of basalt (see on-line database). The pseudosection phase diagram for high Ca is essentially the same as MORB (Fig. 3). Within the diamond stability field the stable assemblage is predicted to be Cpx+Grt+Rt+Coe (class 1) which is the same as produced for MORB, HAB, and THL. The high-Mg protolith composition produces a pseudosection that is nearly identical to AOB (Fig. 3). Qtz is produced near pressures where Pl goes out and Opx is stable at all P–T conditions. The differences are: (1) minor Ky stable at low-P and low-T conditions, and (2) Cpx is ap-

parently not stable at very high-T and low-P conditions. Across the diamondiferous mantle, the stable assemblage is class 1b (Cpx+Grt+Opx+Rt+Coe) which is the same as for AOB. Both altered basaltic protoliths produce quartz at lower pressures and coesite at higher pressures (Fig. 3). Seafloor altered basalts, as represented by the compositions in [12], are not viable as direct protoliths to common mantle eclogite (see also [13]).

5.2. *Residues of high*-P *crystallization*

We have investigated crystallization of basaltic magmas at upper mantle pressures to produce a variety of cumulates. We have generated model cumulate or residue compositions for a variety of basaltic magma compositions using the MELTS program [14]. The model crystallization paths were computed using the same five basalt protolith compositions as parent magma compositions; abbreviated model results are given in the on-line database. All starting compositions were treated as anhydrous and normalized to include only SiO_2, TiO_2, Al_2O_3, FeO(T), MgO, CaO, and Na_2O. The ratio Fe^{2+}/Fe^{3+} of the melt was fixed to the QFM buffer at liquidus conditions. The equilibrium crystallization paths were calculated at a fixed pressure of 2 GPa and used 5°C temperature increments over the temperature interval from liquidus conditions to $>85\%$ crystallization.

Each simulation produces two compositional trends representing: (a) the liquid line of descent attending high-pressure crystallization of the parental melt, and (b) the aggregate composition of the solid assemblage that would accumulate during crystallization. The compositional trends of the accumulated solids and the corresponding residual liquids for the five magma types are shown in a series of oxide plots available as on-line database. Each model scenario involved crystallization, in decreasing abundance, of clinopyroxene and garnet; smaller amounts of feldspar may crystallize late in the crystallization path except in AOB and ANK.

The cumulate solid compositions represent another potential protolith for mantle eclogite. We examined compositions from along the crystal accumulation path for each basalt parent and using the WERAMI option of PERPLEX at the same P–T conditions (1168 K, 4 GPa) on the mantle geotherm as used in previous calculations. Fig. 5 summarizes the range in mantle mineral assemblage resulting from recrystallization of these residues at the fixed P–T condition. We note that the assemblage changes shown in Fig. 5 result strictly from changes in bulk compositions.

These computations lead to several generalities that are independent of the composition of the original magma. All cumulate protoliths associated with low extents of crystallization produce a silica-undersaturated assemblage. Cpx+Grt+Ol ± Opx (class 3/3b) is an assemblage not common in cratonic mantle eclogite. At greater than 60% crystallization, the resulting protoliths produce the more common eclogitic mineral assemblage Cpx+Grt ± Opx (class 2/2b). With increasing crystallization, most cumulate protoliths produce a silica-oversaturated assemblage Cpx+Grt+Coe ± Opx (class 1/1b). The exceptions are

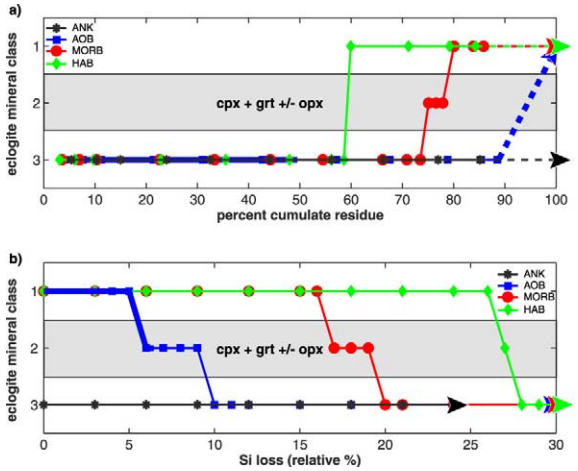

Fig. 5. Classes of eclogite (Table 1 and Fig. 4) deriving from other potential protolith compositions at upper mantle conditions (1168 K, 4 GPa). (a) Classes of mantle eclogite resulting from protoliths produced as cumulates via high-P crystallization of different magma types (MORB, HAB, AOB, and ANK). Simulated cumulates result from 5% to >90% crystallization; dashed lines denote extrapolation of model calculations to 100% crystallization. (b) Classes of eclogite predicted for protoliths produced by loss of silica in basaltic rocks. Thick lines on AOB paths denote regions in which Opx is present; all other paths lack Opx. Mantle eclogite recovered from kimberlite commonly have class 2 mineralogies (shaded field).

protolith compositions that are produced by crystallization of AOB and ANK magmas. All cumulates derived from ANK produce class 3 assemblages over the entire diamondiferous mantle. AOB cumulates also produce class 3 assemblages until 90% crystallization where the cumulates will produce a class 1 (silica-oversaturated) assemblage. In summary, compositions typical of mantle eclogite are indicated by assemblage class 2 (shaded field in Fig. 5). Almost all cumulate paths (except for ANK) can produce class 2 eclogite but only at intermediate to high degrees of crystallization and only over short intervals of crystallization (accumulation). This represents a narrow compositional window of opportunity in which class 2 eclogite can be produced from magma cumulates. Based upon trace element and isotopic data, Taylor et al. [5] have suggested that mantle-type eclogite cannot be the result of igneous crystallization in the mantle.

5.3. Metasomatic processes

One of the obvious differences between the predicted mineralogy of anhydrous basaltic and mantle eclogite is the lack of SiO_2 polymorphs in the latter. The lack of SiO_2 polymorphs must reflect a reduced activity of SiO_2 in mantle eclogite. If mantle eclogite is derived from basalt, then alteration processes must have acted to reduce the activity of SiO_2 in the protolith. Ghent and Coleman [15] suggested that some type C eclogite compositions were modified during transport in ultramafic rocks, producing a nepheline-normative composition. Low SiO_2 activity is common during serpentinization and will also prevail in a mantle dominated by peridotite. Silica loss from basalt is therefore a potential mechanism for producing class 2 eclogite mineral assemblages from common basalt protoliths.

We have modeled this SiO_2 depletion in ANK, AOB, MORB and HAB. Using these starting compositions we produced an array of new compositions by extracting SiO_2 in 1–5% (relative) intervals at 1168 K and 4 GPa. The mineral assemblages are summarized for each protolith as a function of SiO_2 loss (0–30%). Each parent starts with an assemblage equal to the assemblages originally predicted for the individual basalt protoliths (Table 1). All start in class 1 except for ANK which is class 3. However, as SiO_2 is extracted from each basalt parent the resulting mantle mineral assemblage changes for all paths except for ANK which is simply driven to greater degrees of silica undersaturation. All other SiO_2 depletion paths cross the class 2 assemblage. AOB and MORB can easily create class 2 (the normal assemblage) eclogite by SiO_2 loss because it takes relatively low amounts of SiO_2 loss and they reside in the class 2 window for a reasonable range of SiO_2 loss values. HAB requires silica loss of greater than 25% and then quickly crosses to class 3 mineral assemblages. Modest silica loss from MORB is a viable mechanism for producing class 2 eclogites. The loss of silica could occur by fluid-driven advective mass transport during subduction, and in the mantle.

6. Geophysical implications

The main attribute of using a thermodynamic model to describe the equilibrium state of eclogite at mantle conditions is that it provides a complete mineralogical characterization at specific P–T conditions. We use the mineralogy, modal abundances, and mineral compositions to compute in situ P and S wave velocities (V_p, V_s) as a function of protolith composition and depth along the cratonic mantle geotherm using published values for single-crystal elastic moduli for the relevant minerals (see also the version of WERAMI which permits calculation of seismic velocities [4]). Dhaliwal and Graham [16] demonstrated that this approximation reproduced laboratory measurements of V_p in several rock types, including eclogite. Gao et al. [17] compared V_p and V_s measurements to calculations and noted good agreement for crustal rocks and poor agreement for xenolith materials (measured values less than calculated values by up to 15%). The mismatch was attributed to grain boundary alteration and porosity in samples derived from xenoliths, which they suggest are a poor source material in which to measure seismic properties. Calculations of V_p and V_s from mineralogical data described here provide

estimates of the geophysical properties of unaltered mantle eclogite and are also used to explore our capacity to resolve the presence of different classes of eclogite within cratonic mantle lithosphere.

6.1. Calculation of seismic velocities

P and S wave velocities at standard pressure and temperature (300 K, 10^5 Pa) were calculated from isentropic bulk modulus and shear modulus data of isotropic polycrystalline monomineralic aggregates using the Voigt–Ruess–Hill approximation (Table 2) [18]. Elastic constants for pyrope, almandine, grossular, enstatite, ferrosilite, diopside, hedenbergite, forsterite, fayalite, and quartz were taken from Jackson et al. [19], jadeite from Helffrich and Stein [20], and coesite from Gebrande [21]. Sillimanite properties [21] were substituted for kyanite, and magnetite properties [21] adopted for rutile and ilmenite. Bulk and shear moduli were assumed to vary linearly with mole fraction of end-member species in minerals with extensive solid solutions. Values of V_s and V_p at standard pressure and temperature were extrapolated linearly to pressure and temperature of interest (Table 2) assuming $dV_p/dT = -4\times10^{-4}$ km/s/K [22–24], $dV_s/dT = -2\times10^{-4}$ km/s/K [22], $dV_p/dP = 2\times10^{-4}$ km/s/MPa ([22], [24], and $dV_s/dP = 1\times10^{-4}$ km/s/MPa [22].

6.2. Velocity profiles for eclogite in mantle lithosphere

Fig. 6 illustrates variations in seismic velocity (V_s, V_p) and Poisson's ratio at mantle conditions as a function of depth for a subset of protolith compositions chosen to span all three mineral classes (Tables 1). The values calculated for the mantle conditions 1168 K and 4 GPa (Table 2) are also are compared to measured values of V_p and V_s extracted from the literature (Fig. 7). Calculated V_p and V_s for eclogite vary from 4.9 to 5.1 and 8.6 to 9.0, respectively, and are consistently higher than those measured. We attribute this mismatch to alteration of eclogite xenoliths (cf. [15]). Both measured and calculated V_p and V_s of eclogite, however, are consistently higher than those of peridotite and crustal rocks. The distinctive geophysical signature may therefore be useful for constraining the proportion of eclogite from estimates of seismic velocities of mantle lithosphere [23]. Poisson's ratio of eclogite is almost constant (0.262–0.265) and overlaps that of

Table 2
Seismic properties calculated for model eclogite based on mineral assemblages and mineral compositions predicted for different protoliths

Protolith	Class[a]	Standard state[b]				Mantle P–T[c]			
		V_p	V_s	V_p/V_s	σ	V_p	V_s	V_p/V_s	σ
ACA	1	8.41	4.80	1.754	0.259	5.02	8.87	1.765	0.264
HAB	1	8.54	4.86	1.756	0.260	5.09	8.99	1.767	0.264
MORB	1	8.41	4.79	1.757	0.260	5.02	8.87	1.768	0.265
AMG	1b	8.47	4.83	1.753	0.259	5.06	8.93	1.764	0.263
AOB	1b	8.31	4.73	1.758	0.261	4.96	8.77	1.769	0.265
MORB 17%	2	8.53	4.86	1.756	0.260	5.08	8.98	1.767	0.264
MORB 19%	2	8.55	4.87	1.755	0.260	5.1	9.00	1.766	0.264
AOB 6%	2b	8.38	4.77	1.759	0.261	4.99	8.84	1.770	0.266
MORB 20%	3	8.57	4.88	1.755	0.260	5.11	9.02	1.766	0.264
ANK	3	8.17	4.65	1.756	0.260	4.88	8.63	1.767	0.265
AOB 21.5%	3b	8.14	4.65	1.75	0.257	4.88	8.59	1.761	0.262
Mean		4.79	8.41	1.76	0.26	5.02	8.86	1.77	0.26
1 S		0.08	0.15	0.003	0.001	0.08	0.15	0.003	0.001

Properties include compressional (V_p) and shear ($V_{s)}$ wave velocities and Poisson's ratio (σ). 1 S = 1 standard deviation.
[a] Mineralogical classes defined in Table 1 and Fig. 4.
[b] Properties of model eclogite at standard state conditions (300 K and 0.1 MPa).
[c] Properties of model eclogite at mantle conditions (1168 K, 4 GPa).

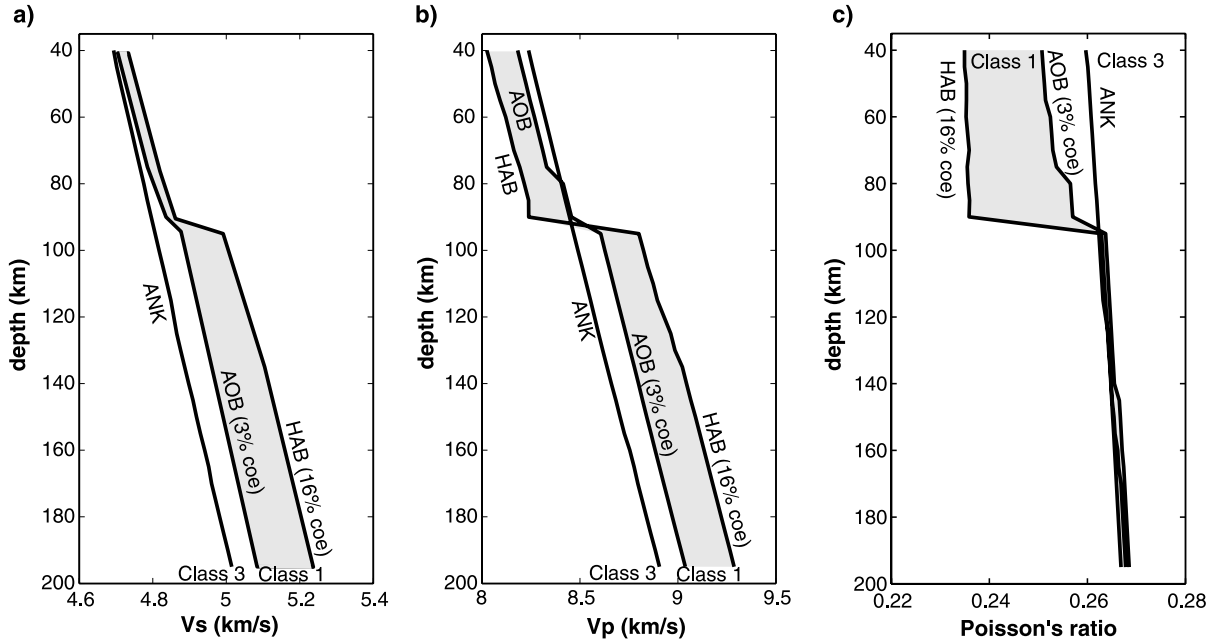

Fig. 6. Calculated seismic properties for eclogitic mineral assemblages for a subset of protoliths are plotted as a function of depth along the mantle geotherm. The properties calculated for mantle conditions along the geotherm include: (a) V_s (km/s), (b) V_p (km/s), and (c) Poisson's ratio. Class 1 assemblages are silica-oversaturated and show a pronounced step that is coincident with the transition from quartz to coesite. Class 3 (e.g., ANK) lacks Qtz/Coe and features a more or less continuous rise in seismic velocities with depth. Class 2 rocks are not represented but have intermediate seismic properties. Poisson's ratio shows little variation at depths greater than the Qtz–Coe transition.

most other mantle rocks (Fig. 7). At 1168 K, 4 GPa, there is no systematic difference in seismic properties between eclogite mineral classes: variation of V_s, V_p and Poisson's ratio in class 3 exceeds the combined range of classes 1 and 2 (Fig. 7, inset). Regional seismic surveys, therefore, cannot distinguish between eclogite mineral classes, at least within the diamond stability field. Class 1 eclogite could be detected at shallower levels, however, because of the unusual seismic properties of Qtz [18]. Calculated seismic velocities along the mantle geotherm for class 1 eclogite are shown as the gray field in Fig. 6. The sharp increase in V_s and V_p at 90 km depth corresponds to the Qtz–Coe phase transition, and the magnitude of the increase is roughly proportional to Qtz and Coe content. Qtz/Coe content and seismic velocities of MORB and THL are intermediate between those of HAB and AOB. The presence of eclogite derived from unmodified basalt compositions might therefore be detectable from contrasts in V_p and V_s at about 90 km depth in regional seismic surveys.

7. Conclusions

The mineralogy and geophysical properties of eclogite are dictated by bulk composition and P–T conditions of formation. Therefore, for a specific geotherm, variations in eclogite mineralogy must reflect the controls of bulk composition and hence the protolith. Here we have used thermodynamic models to explore the mineralogical and geophysical variations of eclogite within cratonic mantle lithosphere as a function of several types of protolith.

The calculated modal mineralogy of eclogite changes little below about 90 km depth along a Slave geotherm. Within the diamond stability field of cratonic mantle lithosphere, eclogite has a single mineral assemblage. The mineral assemblage

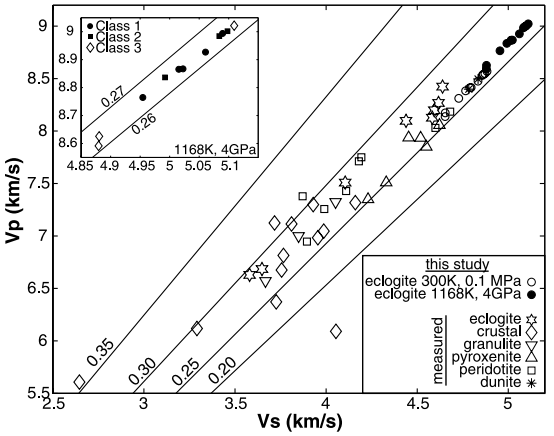

Fig. 7. Calculated seismic properties for model eclogite plotted as V_p vs. V_s (km/s) and compared to values for common mantle and crustal rocks [17,25–27]). Calculated values are for model eclogite classes at standard state (open circles) and mantle P–T conditions (solid). Measured seismic properties of rocks are contoured as Poisson's ratio (solid lines). Inset uses expanded scale to show V_p and V_s variations predicted for individual eclogite classes as defined in this paper (Table 1). Model classes of eclogite have predicted Poisson's ratios between 0.26 and 0.27.

varies with protolith composition and we recognize three basic classes (Table 1): (1) a silica-oversaturated assemblage indicated by the presence of coesite, (2) a silica-saturated assemblage distinguished by the absence of coesite and olivine, and (3) a silica-undersaturated assemblage containing olivine.

Within the diamond stability field of the cratonic mantle, Ky-bearing eclogite is stable only in protoliths featuring extreme Al enrichment. Isolated megacrysts or inclusions of Ky in diamondiferous kimberlite may represent xenocrysts deriving from the graphite stability field. In contrast, some eclogite from ultra-high-pressure environments form along cooler geotherms and feature Ky ± diamond.

Class 2 eclogite is the most common class of eclogite in cratonic mantle lithosphere. Normal basalt compositions and compositions we have chosen as representative of seafloor altered basalt cannot serve as protolith to class 2 eclogite. Class 2 eclogite is interpreted as resulting from protoliths resulting from cumulates of metaluminous, subalkaline magmas or silica metasomatism operating on subducted basalt. The former process can produce compositions that will result in class 2 eclogite assemblages but only over very restricted ranges of crystallization. Thus, a cumulate igneous origin by crystallization of basaltic melts is unlikely but cannot be ruled out. Metasomatic processes seem feasible because the intrinsically low silica activity in peridotitic mantle offers a clear rationale for the efficient extraction of silica from the volumetrically subordinate but more more siliceous basalts as represented by THL, MORB, AOB.

The calculated and measured velocities of model eclogite in cratonic mantle lithosphere are higher than corresponding velocities for peridotite and most crustal rocks and therefore may be distinctive in regional seismic surveys. Poisson's ratio varies little between eclogite mineral classes and between eclogite and most other mantle rocks. The only eclogite that might be specifically identified in seismic surveys is the oversaturated assemblage (class 1). The Qtz–Coe transition produces a sharp change in V_p–V_s at about 90 km depth along the ambient mantle geotherm.

Acknowledgements

This research is supported by NSERC through Discovery Grants to all authors. We acknowledge critical discussions with Maya Kopylova, Fred Cook, and Jim Nicholls. Jamie Connolly, Bernie Wood and an anonymous reviewer are thanked for critically reviewing the manuscript.*[BW]*

References

[1] M.G. Kopylova, J.K. Russell, H. Cookenboo, Petrology of peridotite and pyroxenite xenoliths from the Jericho kimberlite: implications for the thermal state of the mantle beneath the Slave craton, northern Canada, J. Petrol. 40 (1999) 79–104.

[2] M.G. Kopylova, J.K. Russell, H.O. Cookenboo, Mapping the lithosphere beneath the north central Slave craton, in: J.J. Gurney, S. Richardson (Eds.), Proceedings of the 7th International Kimberlite Conference, Red Roof Design, Capetown, 1999, pp. 468–479.

[3] T.J.B. Holland, R. Powell, An internally consistent ther-

modynamic dataset for phases of petrological interest, J. Metamorph. Geol. 16 (1998) 309–343.
[4] J.A.D. Connolly, Multivariable phase diagrams: an algorithm based upon generalized thermodynamics, Am. J. Sci. 290 (1990) 666–718.
[5] L.A. Taylor, G.A. Snyder, R. Keller, D.A. Remley, M. Anand, R. Wiesli, J. Valley, N.V. Sobolev, Petrogenesis of group A eclogites and websterites evidence from the Obnazhennaya kimberlite, Yakutia, Contrib. Mineral. Petrol. 145 (2003) 424–443.
[6] D.H. Green, A.E. Ringwood, An experimental investigation of the gabbro to eclogite transformation and its petrologic applications, Geochim. Cosmochim. Acta 31 (1967) 767–833.
[7] R. Kretz, Symbols for rock-forming minerals, Am. Mineral. 68 (1983) 277–279.
[8] J.K. Russell, M.G. Kopylova, A steady-state conductive geotherm for the north-central Slave, Canada: Inversion of petrological data from the Jericho kimberlite pipe, J. Geophys. Res. 104 (1999) 7089–7101.
[9] J.K. Russell, G.M. Dipple, M.G. Kopylova, Heat production and heat flow in the mantle lithosphere to the Slave craton, Canada, Phys. Earth Planet. Inter. 123 (2001) 27–44.
[10] V.S. Shatsky, N.V. Sobolev, M.A. Vavilov, Diamond-bearing metamorphic rocks of the Kokchetav Massif (northern Kazakhstan), in: R.G. Coleman, X. Wang (Eds.), Ultrahigh Pressure Metamorphism, 1995, pp. 427–455.
[11] R.G. Berman, Internally consistent thermodynamic data for minerals in the system Na_2O-K_2O-CaO-MgO-FeO-Fe_2O_3-Al_2O_3-SiO_2-TiO_2-H_2O-CO_2, J. Petrol. 29 (1988) 445–522.
[12] S.E. Humphris, G. Thompson, Hydrothermal alteration of oceanic basalts by seawater, Geochim. Cosmochim. Acta 42 (1978) 107–125.
[13] J.A.D. Connolly, D.M. Kerrick, Metamorphic controls on seismic velocity of subducted oceanic crust at 100–250 km depth (0.3 Mb), Earth Planet. Sci. Lett. 204 (2002) 61–74.
[14] M.S. Ghiorso, R.O. Sack, Chemical mass transfer in magmatic processes IV: A revised and internally-consistent thermodynamic model for the interpolation and extrapolation of liquid-solid equilibria in magmatic systems at elevated temperatures and pressures, Contrib. Mineral. Petrol. 119 (1995) 197–212.
[15] E.D. Ghent, R.G. Coleman, Eclogites from southwestern Oregon, Geol. Soc. Am. Bull. 84 (1973) 2471–2488.
[16] H. Dhaliwal, E.K. Graham, A comparison of theoretical rock models with laboratory data, Tectonophysics 188 (1991) 373–383.
[17] S. Gao, H. Kern, Y.-S. Liu, S.-Y. Jin, T. Popp, Z.-M. Jin, J.-L. Feng, M. Sun, Z.-B. Zhao, Measured and calculated seismic velocities and densities for granulites from xenolith occurrences and adjacent exposed lower crustal sections: A comparative study from the North China craton, J. Geophys. Res. 105 (2000) 18965–18976.
[18] C.R. Bina, G. Helffrich, Calculation of elastic properties from thermodynamic equation of state principles, Annu. Rev. Earth Planet. Sci. 20 (1982) 527–552.
[19] I. Jackson, R.L. Rudnick, S.Y. O'Reilly, C. Bezant, Measured and calculated elastic wave velocities for xenoliths from the lower crust and mantle, Tectonophysics 173 (1990) 207–210.
[20] G. Helffrich, S. Stein, Study of the structure of the slab-mantle interface using reflected and converted seismic waves, Geophys. J. Int. 115 (1993) 14–40.
[21] H. Gebrande, Elastic wave velocities and constants of elasticity of rocks and rock forming minerals, in: G. Angenheister (Ed.), Physical Properties of Rocks, vol. 1b, Springer-Verlag, New York, 1982, pp. 1–99.
[22] H. Kern, Elastic wave velocities and constants of elasticity of rocks at elevated pressures and temperatures, in: G. Angenheister (Ed.), Physical Properties of Rocks, vol. 1b, Springer-Verlag, New York, 1982, pp. 99–140.
[23] N.I. Christensen, W.D. Mooney, Seismic velocity structure and composition of the continental crust: a global view, J. Geophys. Res. 100 (1995) 9761–9788.
[24] R.L. Rudnick, D.M. Fountain, Nature and composition of the continental crust: a lower crustal perspective, Rev. Geophys. 33 (1995) 267–309.
[25] N.I. Christensen, Poisson's ratio and crustal seismology, J. Geophys. Res. 101 (1996) 3139–3156.
[26] M.G. Kopylova, J.K. Russell, N.I. Christensen, Composition and fabric of the N. Slave eclogite as evidence for mantle metasomatism in Mantle Lithosphere and Lithoprobe: Views of continental evolution from the bottom up, Lithoprobe workshop III, October 27–29, 2001, Banff, Canada, Lithoprobe Report No. 81, pp. 61–70.
[27] C. Long, N.I. Christensen, Seismic anisotropy of South African upper mantle xenoliths, Earth Planet. Sci. Lett. 179 (2000) 551–565.